inorganics

MDPI

Article

Exploring the Interaction of Pyridine-Based Chalcones with Trinuclear Silver(I) Pyrazolate Complex

Arina Olbrykh [1,2], Aleksei Titov [1], Alexander Smol'yakov [1,3], Oleg Filippov [1] and Elena S. Shubina [1,*]

[1] A. N. Nesmeyanov Institute of Organoelement Compounds, Russian Academy of Sciences, Vavilov Str. 28, 119334 Moscow, Russia; arinaolbr@gmail.com (A.O.); tit@ineos.ac.ru (A.T.); rengenhik@gmail.com (A.S.); h-bond@ineos.ac.ru (O.F.)
[2] Higher Chemical College, Mendeleev University of Chemical Technology of Russia, Miusskaya Sq. 9, 125047 Moscow, Russia
[3] Basic Department of Chemistry of Innovative Materials and Technologies, G. V. Plekhanov Russian University of Economics, Stremyanny per. 36, 117997 Moscow, Russia
* Correspondence: shu@ineos.ac.ru

Abstract: The investigation of the interaction of cyclic trinuclear silver(I) pyrazolate $[AgPz]_3$ (Pz = 3,5-bis(trifluoromethyl)pyrazolate) with pyridine-based chalcones (anthracen-9-yl and phenyl-substituted ones) has been performed by IR-, UV-vis, and NMR spectroscopies in the solution. The carbonyl group participates in coordination with metal ions in all complexes. However, the network of π-π/M-π non-covalent intermolecular interactions mainly influences complex formation. The spectral data suggest retaining the structures for all studied complexes in the solution and solid state. E-Z isomerization in the case of anthracene-containing compounds significantly influences the complexation. E-isomer of chalcones seeks the planar structure in the complexes with $[AgPz]_3$. In contrast, the Z-isomer of chalcone demonstrates the chelating coordination of O- and N atoms to silver ions. The complexation of anthracene-containing chalcones allows the switching of the emission nature from charge transfer to ligand-centered at 77 K. In contrast, phenyl-substituted chalcone in complex with macrocycle demonstrates that the emission significantly shifted (Δ = ca. 155 nm) to the low-energy region compared to the free base.

Keywords: cyclic trinuclear complex; pyrazolate adducts; silver(I); non-covalent interactions; photoluminescence

check for updates

Citation: Olbrykh, A.; Titov, A.; Smol'yakov, A.; Filippov, O.; Shubina, E.S. Exploring the Interaction of Pyridine-Based Chalcones with Trinuclear Silver(I) Pyrazolate Complex. *Inorganics* **2023**, *11*, 175. https://doi.org/10.3390/inorganics11040175

Academic Editor: Antonio Laguna

Received: 31 March 2023
Revised: 12 April 2023
Accepted: 17 April 2023
Published: 21 April 2023

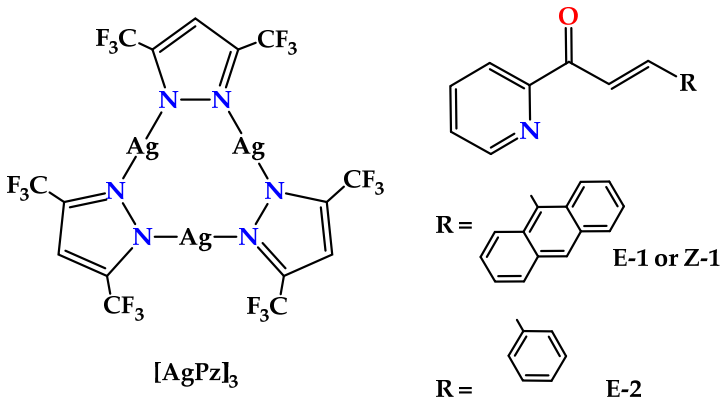
Copyright: © 2023 by the authors. Licensee MDPI, Basel, Switzerland. This article is an open access article distributed under the terms and conditions of the Creative Commons Attribution (CC BY) license (https://creativecommons.org/licenses/by/4.0/).

1. Introduction

Non-covalent intermolecular interactions are one of the important driving forces in coordination and organometallic chemistry [1–3]. Hydrogen or halogen bonding, π−π stacking, and other types of donor-acceptor interactions lead to the formation of supramolecular aggregates determining their structures and properties [4–7]. Complexes possessing metallophilic interactions has been of rising interest in the last decade. The ability of such complexes to realize the metal-involved inter- or intra-molecular interactions, allowing the formation of the coordination compounds and supramolecular aggregates, determines their properties and practical use in areas such as photoluminescence [8–14], gas sensing, molecules recognition [8–11,15–18], and catalysis [5–7,19–21]. Weak intermolecular interactions play an important role in the chemistry of cyclic trinuclear coinage metal pyrazolate complexes [22–24]. Firstly, Dias et al. demonstrated the ability of this type of compound for infinite stacks via intermolecular metal-metal interactions [25,26]. Trinuclear metal pyrazolates are polydentate Lewis acids and interact with bases of wide nature and structures. For example, it demonstrates the significant affinity to compounds possessing π-electronic systems, such as alkenes, arenes, alkynes, etc. [16,27–32]. From another hand, trinuclear metal pyrazolates form stable complexes with boron hydrides or halide substituents/ligands [33–37]. Interaction of this class of compound with P- or N-donor

ligands allows the rearrangement of the central core with the formation of di-, tri-, tetra-, or pentanuclear cores [15,38–44]. Our studies of the host-guest complexes of the macrocyclic coinage metal pyrazolates with ketones or isocoumarines possess their coordination via the oxygen atom of the C=O group and demonstrate the formation of 1:1 complexes in the solution. The preferable μ^3-coordination of the O atom to three metal ions has been observed in the crystal [45,46]. Based on the ability of trinuclear metal pyrazolates to form complexes with compounds possessing carbonyl groups and basic nitrogen atoms, the pyridine-containing chalcones were chosen as agents for the complexation with silver(I) trinuclear macrocycle ($[AgPz]_3$, Pz = 3,5-bis(trifluoromethyl)pyrazolate anion). The ability of pyridine-chalcones to chelate metal ions is known because this class of compound has been suggested as a structural analog of bipyridine-type ligands [47–50].

Herein, we report the investigation complexation of trinuclear silver(I) 3,5-bis(trifluoromethyl) pyrazolate $[AgPz]_3$ with pyridine-based chalcones containing anthracenyl or phenyl substituents. In the case of anthracenyl-substituted compound, two isomers E/Z have been studied (E-3-(anthracen-9-yl)-1-(pyridin-2-yl)prop-2-en-1-one—E-**1**, and Z-3-(anthracen-9-yl)-1-(pyridin-2-yl)prop-2-en-1-one—Z-1; Scheme 1). In contrast, the phenyl-substituted analog demonstrates only stability of E-isomer (E-3-phenyl-1-(pyridin-2-yl)prop-2-en-1-one, E-**2**) substituents (Scheme 1). This work aimed to reveal the center of coordination, composition, and structures of complexes obtained, and the photoluminescence properties.



Scheme 1. Chemical structures of cyclic silver(I) pyrazolate and chalcones **1**-**2**.

2. Results and Discussions

Pyridine-based chalcones possess various potential centers of coordination to the silver(I) pyrazolate complex $[AgPz]_3$: carbonyl-group, pyridine-fragment, or extended π-electronic systems within a double bond and aromatic substituents. The complexation of $[AgPz]_3$ in solution was investigated using IR, UV-vis, and NMR spectroscopy. The interaction of $[AgPz]_3$ with bases is preferable in low-polar solvents. The investigation of the complexation was performed in CCl_4 based on the better solubility of initial chalcones. Compounds E-**1** and E-**2** show intense bands of the ν(C=O) stretching vibration at 1677 and 1675 cm^{-1}, respectively (Figure 1). Chalcones also demonstrates the intense bands of C=C double bond stretching vibrations (ν(C=C)) at 1603 and 1610 cm^{-1}, for E-**1** and E-**2** correspondingly. The titration of chalcones solution in CCl_4 with $[AgPz]_3$ leads to a decrease in the intensity of initial $\nu(C=O)^{free}$ and $\nu(C=C)^{free}$ bands and an increase in the new low-frequency bands $\nu(C=O)^{bond}$ (1650 and 1655 cm^{-1}) and $\nu(C=C)^{bond}$ (1590 and 1591 cm^{-1}). The participation of the functional group in coordination with metal ions is accompanied by the arising of low-frequency bands in the IR spectrum, demonstrating that the carbonyl group and C=C double bond participate in the interaction with macrocycle $[AgPz]_3$.

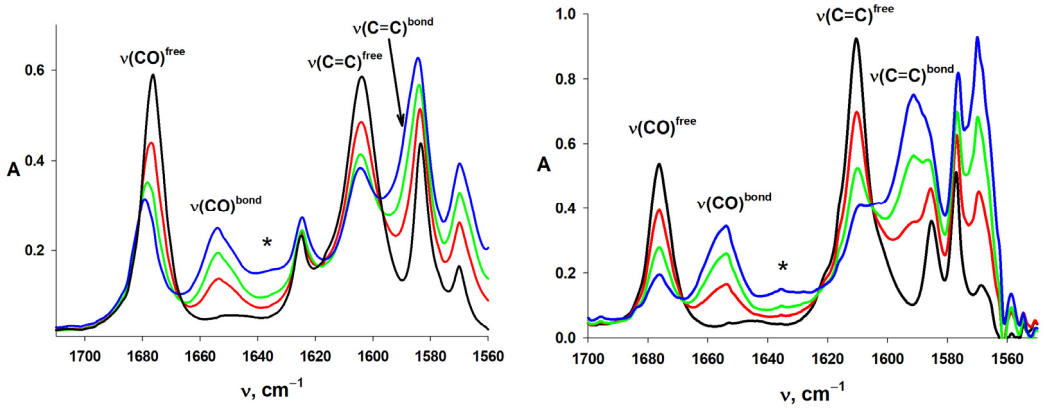
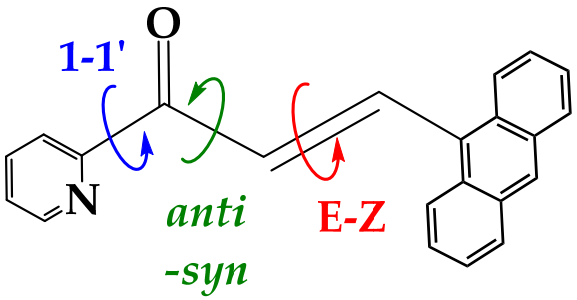


Figure 1. The IR spectra of E-**1** (**a**) and E-**2** (**b**), (c = 0.015, d = 1 mm, black line), in the presence of 0.5 (red), 1 (green), and 2 (blue) equivalents of $[AgPz]_3$; CCl_4, 298 K. * $\delta(C\text{-}N)^{[AgPz]3}$.

E-**1** and E-**2** have one, relatively easy-to-isomerize, double bond. These compounds also possess two single C-C(O) bonds allowing the formation of the eight isomers/rotamers (Scheme 2; also see Scheme S1 in SI).



Scheme 2. Possible rotations in chalcone **1**.

In the case of anthracene-containing chalcone, all possible isomers/rotamers are within the 5.2 kcal/mol Gibbs energy range, while six of them are in the 2.8 kcal/mol range. Due to the various local surroundings of the C=O group, it possesses different IR spectral patterns. This includes both band position and intensity (Table 1).

Table 1. Calculated CO and CC frequencies (in cm^{-1}, scaled by 0.95 [51], intensities (in km/mol), and relative energies of isomers (in kcal/mol).

	ΔG^{298}	ν(C=O) (A)	ν(C=C) (A)
anti-E-1	0.0	1682 (269) [a]	1611 (573) [b]
anti-E-1′	+2.7	1691 (278) [a]	1613 (553) [b]
syn-E-1	+2.1	1658 (700)	1638 (118)
syn-E-1′	+3.7	1671 (685)	1634 (159)
anti-Z-1	+2.8	1690 (287) [a]	1637 (84); 1627 (5)
anti-Z-1′	+5.2	1696 (303) [a]	1637 (112); 1627 (4)
syn-Z-1	+2.0	1671 (601)	1632 (27); 1625 (11)
syn-Z-1′	+2.7	1680 (591)	1631 (26); 1624 (21)

[a] highly mixed with ν(C=C); [b] highly mixed with ν(C=O).

The frequencies of ν(C=O) are systematically higher for the Z-isomer, while intensities are higher for the *syn* C=C-C(O) rotamer (CH-syn-to-CO). The ν(C=C) is located at the same wavenumbers, except for the *anti*-E-1 and *anti*-E-1′ where it is ca. 20 cm^{-1} lower

and of rather high intensity. The pyridine rotation does not lead to significant changes in the ν(C=O)/ν(C=C) intensities ratios after shifting ν(C=O) by ca. 10 cm^{-1} higher in the rotamer without $CH^{Py}\cdots O$ contact. Since this kind of rotamer is systematically higher by energy, it could be excluded from further consideration in the solution.

Therefore, free E-**1** adopts *anti*-E geometry in the solution evidenced by the high-intensity ν(C=C) band in the IR spectra, comparable to those of ν(C=O). Since ν(C=C) and ν(C=O) are highly mixed at this geometry, the complex formation leads to low-frequency shifts of both bands in the spectra.

The complexation in the case of anthracene-containing chalcone E-**1** was accompanied by a change of the solution color from orange to orange-red. The interaction of chalcones with silver pyrazole complex has been investigated by UV-vis spectroscopy. Compound E-**1** shows a broad band with a vibronic structure in the UV-vis spectrum (340, 364, 386, 413, and 440 nm; Figure 2). It could be assigned to charge transfer from the anthracene fragment to the pyridine-carbonyl fragment (ILCT) and π→π* transitions within the extended aromatic system of anthracene. The titration of E-**1** solution in CCl_4 with silver(I) complex leads to the decrease in the initial bands and arising of a new low-energy band at ca. 503. Increasing the amount of $[AgPz]_3$ leads to a further decrease in the initial bands and an increase in the new band, demonstrating the complexation.

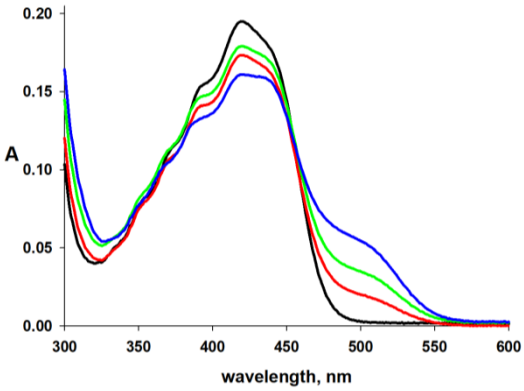


Figure 2. The UV-vis spectra of E-**1** (c = 0.015 M, d = 0.047 mm, black line) in the presence of 0.5 (red), 1 (green), and 2 (blue) equivalents of $[AgPz]_3$; CCl_4, 298 K.

In contrast, phenyl-substituted chalcone E-**2** does not possess charge transfer and exhibits only π→π* transitions demonstrating high-energy bands centered at ca. 320 nm (Figure S16). The titration of E-**2** solution with $[AgPz]_3$ leads to the same behavior: the intensity of a free chalcone decrease and a new low-energy band increase.

The compositions of complexes were determined by Job's method in the example of chalcone E-**1**. It was shown using IR and UV-vis spectroscopy (see supporting information) that a complex containing one molecule of E-**1** per one molecule of macrocycle at molar ratios from 7:1 to 1:7 is formed in the CCl_4 solution. Thus, the complexes could be formulated as {E-**1**·$[AgPz]_3$} (E-**1Ag**) and {E-**2**·$[AgPz]_3$} (E-**2Ag**).

Crystallization from the equimolar solution (E-**1**/$[AgPz]_3$ = 1/1) in CCl_4 at ambient conditions by slow solvent evaporation (air, room temperature, unprotected from light) led to the formation of crystals suitable for XRD experiments. Interestingly, the Z-form of chalcone **1** has been established in the complex obtained (Figure 3, Scheme S3). It is known that anthracene-containing chalcones undergo E-Z isomerization under ambient light [52]. Complex obtained could be formulated as {(Z-**1**)·$[AgPz]_3$} (Z-**1Ag**, Z-1 = anti-Z-1′). Complex Z-**1Ag** contains one molecule of chalcone per one molecule of $[AgPz]_3$. The oxygen atom of the carbonyl group and the nitrogen atom in the pyridine fragment chelated one silver atom in the trinuclear core. The Ag1 … O1 and Ag1 … N7 bonds are 2.611(3) and 2.403(4) Å, respectively. There is a shortened contact Ag2 … O1 (2.951(4) Å) in complex Z-**1Ag**. The carbonyl group oxygen atom and pyridine nitrogen atom chelate

a single silver ion in the trinuclear complex, leading to a tetracoordinate environment. A practically linear (175.6°) N^{Pz}-Ag-N^{Pz} angle in free $[AgPz]_3$ adducts [53] is bent to 142.8° in complex Z-**1Ag**. Consequently, corresponding N^{Pz}-Ag bonds increase to 2244 and 2168 Å (typically ca. 2.1 Å in a free $[AgPz]_3$) [53]. The corresponding Ag . . . O and Ag . . . N bonds are in a similar range compared to the complexes of silver(I) pyrazolates with carbonyl compounds or diimines [42,43,45,46].

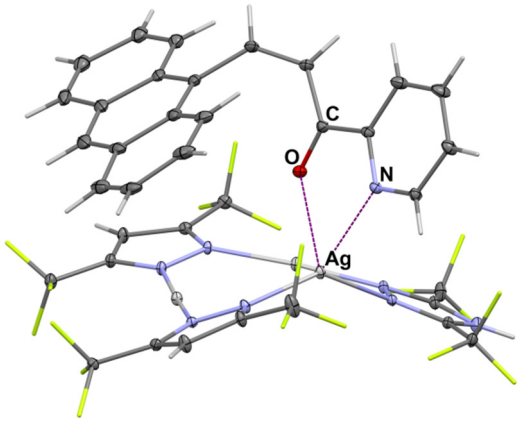


Figure 3. XRD structure of complex Z-**1Ag** with thermal ellipsoids set at the 15% probability level. Hydrogen and Fluorine atoms are sticks for clarity.

Supramolecular packing of complex Z-**1Ag** is realized via a network of Ag-π^{antra} (3.317–3.401 Å, antra = anthracene) and π^{Py}-π^{CO} (3.328) intermolecular interactions. The F-F, F-H, and H-π^{Pz} contacts are also presented in supramolecular packing (Figure 4).

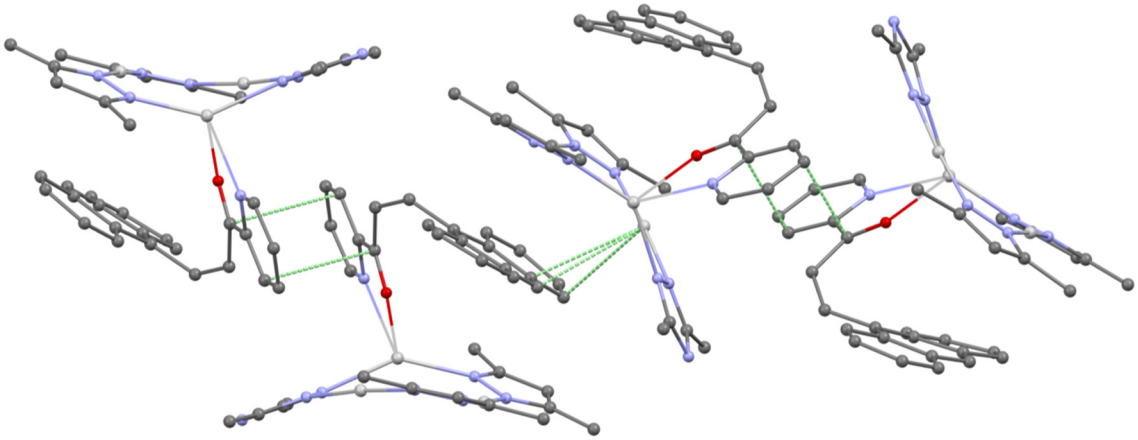
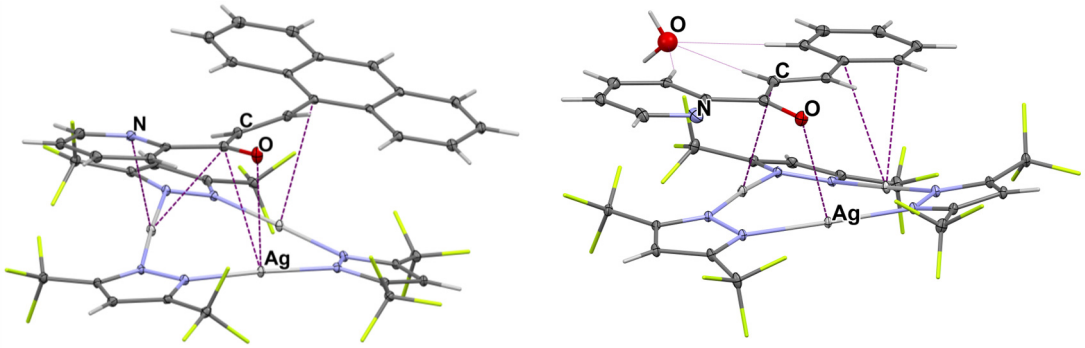


Figure 4. Fragment of a supramolecular packing of complex Z-**1Ag** demonstrating Ag-π^{antra} (3.317–3.401 Å) and π^{Py}-π^{CO} contacts.

Considering that E-**1** could be easily converted to Z-**1**, the crystals of complexes $[AgPz]_3$ with chalcones E-**1** and E-**2** were obtained from equimolar reagents CCl_4 solution after staying at −5 °C and being protected from the light with an aluminum foil. In a crystal, complexes E-**1Ag** and E-**2Ag** contain one chalcone per macrocycle. These complexes demonstrate significant differences in the complex Z-**1Ag** described above. Both E-**1** and E-**2** possess almost planar geometry (Figure 5, Scheme S2). The carbonyl group participates in coordination with the silver ions. However, the Ag-O distances are significantly longer (3.345(3) and 2.887(4) Å) than that in **Z-1Ag**, evidencing weaker interactions. Moreover, a silver ion in complex E-**1Ag** also interacts with a carbon atom in the C=O group (3.367(4) Å). There are also weak N^{Py} . . . Ag (3.110(3) Å), Ag . . . $C^{C=C}$ (3.468(4) Å), and Ag . . . C^{Antra}

(3.463(4) Å) contacts in complex E-**1Ag**. It should be noted, that this complex possesses steric repulsions demonstrating their low stability. Chalcone E-**1** is the most favorable *anti*-E-1 conformer in complex E-**1Ag** (*vide supra*) correlating with DFT calculations. These results demonstrate the similar structures of complexes in the solution and the solid state. In contrast, E-**2Ag** shows very tight packing with significantly shorter Ag-C contacts. For example, Ag2 interacts with Ph substituent (3.087(4), 3.264(4) Å) and Ag3 with one carbon atom of C=C double bond (Ag . . . C is 3.306(3) Å). The presence of several shortened contacts with different fragments of E-**2** leads to higher stability of complex E-**2Ag**. It should be noted that the water molecule is also observed in the structure of E-**2Ag** leading to the alternative *anti*-E-**2′** conformation of chalcone. Although pyridine ligand is already rotated into position to form a chelate complex with silver, as in Z-**1Ag**, there is no such interaction in E-**2Ag**, additionally evidencing that pyridine rotation is only due to intermolecular interactions with water.



(**a**) (**b**)

Figure 5. XRD structures of complexes **E-1Ag** (**a**) and **E-2Ag** (**b**) with thermal ellipsoids set at the 15% probability level. Hydrogen and fluorine atoms are sticks for clarity.

Supramolecular packing of complexes **E-1Ag** and E-**2Ag** is also realized via the network of Ag-π^{antra}, π-π, F-F, F-H, and H-π intermolecular interactions.

Based on the possibility of easy E-Z isomerization of **1**, we investigated the interaction of $[AgPz]_3$ with Z-**1** in the solution at conditions similar to that for E-**1**. Z-isomer has been obtained by UV irradiation from its solution in $CHCl_3$. Chalcone Z-**1** shows an intense band of the ν(C=O) stretching vibration at 1677 in the IR spectrum (Figure 6). The intensity of $\nu(C=C)^{free}$ (1610 cm^{-1}) in this case is lower. Although the DFT predicts that *syn*-Z-**1** is 0.7 kcal·mol^{-1} preferred over *anti*-Z-**1**, the spectral pattern (retention of ν(C=O) intensity compared to *anti*-E-1, and ν(C=C) intensity being only 2–3 times lower than that of ν(C=O), and it is not one order of magnitude lower) suggests that, namely, *anti*-Z-**1** conformer predominate in the solution. Adding $[AgPz]_3$ to the solution of **Z-1** leads to the initial $\nu(C=O)^{free}$ band decrease and increase in the new low-frequency band at 1642 cm^{-1}, corresponding to the coordinated silver atoms carbonyl group. In this case, the $\Delta\nu$(C=O) shift is 43 cm^{-1} which is larger than that observed for a complex with *anti*-E-**1** ($\Delta\nu$ = 27 cm^{-1}). This data demonstrates the possibility of different coordination of pyridine-based chalcones to $[AgPz]_3$ in the solution. The intensity of the $\nu(C=C)^{free}$ does not exhibit significant dependence on complexation, since in the *anti*-Z-1 it is not mixed with the ν(C=O). Moreover, there is no low-frequency $\nu(C=C)^{bond}$ band observed in the spectrum. Probably, $\nu(C=C)^{in\ compl}$ could be located near the $\nu(C=C)^{free}$ forming a whole spectral shape.

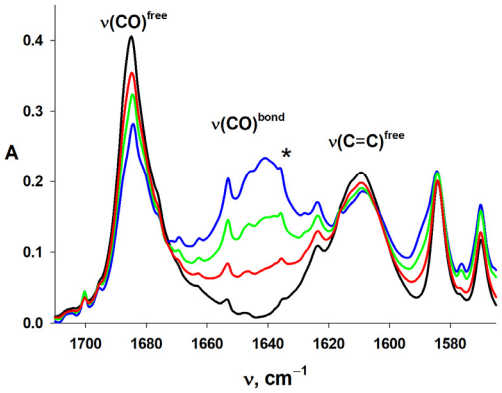


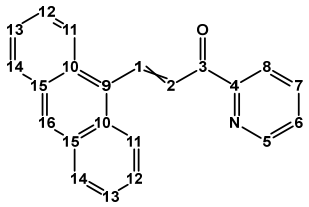
Figure 6. The IR spectra of chalcones Z-**1**, (c = 0.015 M, d = 1 mm, black line) in the presence of 0.5 (red), 1 (green), and 2 (blue) equivalents of $[AgPz]_3$; CCl_4, 298 K. * $\delta(C\text{-}N)^{[AgPz]3}$.

The interaction of Z-**1** with $[AgPz]_3$ is also accompanied by the changing of color. The initial orange solution of Z-**1** became red-orange upon the addition of the macrocycle. The crystallization from the saturated solution of chalcone Z-**1** with macrocycle $[AgPz]_3$, an equimolar reagents ratio, leads to the formation of previously described complex **Z-1Ag**, which was obtained by the crystallization of chalcone **1** (E-isomer) under the light.

Investigation of the $[AgPz]_3$ interactions with Z-1 and E-1 in the solution was carried out using ^1H and ^{13}C NMR spectroscopy in CCl_4/C_6D_6 mixture (v/v=9/1) (Figures S1–S8). The resonances of all protons in Z-**1 and** E-**1** undergo a high-field shift in the presence of the macrocycle. The main differences have been observed in the ^{13}C NMR spectra. The carbonyl group carbon atom resonance of E-**1** does not possess any changes upon the addition of $[AgPz]_3$. In contrast, the peak for the carbon atom of the CO group Z-**1** undergoes a low-field shift by 0.66 ppm upon adding even a 0.5 equivalent of silver macrocycle at room temperature. The resonances of carbon atoms (numbers 4–8 in Table 2) in the pyridine fragment of E-**1** undergo only a low-field shift. The resonances of C4 and C6-7 in the pyridine fragment of chalcone Z-**1** show the high-field shifts demonstrating the participation of this fragment in coordination. Carbon atoms in anthracenyl fragments are mostly shifted to the high-field in **E-1Ag**, but there are only two carbons in anthracene substituents of **Z-1** demonstrating the same behavior. The low-field shift of resonances of the carbon atoms in aromatic fragments demonstrates the presence of coordination [54].

Finally, we have investigated the photophysical properties of the complexes obtained in the solid state. It should be noted that free chalcones Z-**1** and E-**1**, as well as their complexes **E-1Ag**, and **Z-1Ag**, have not demonstrated isomerization in the solid state. Anthracene-containing chalcones exhibit unstructured broad bands of charge-transfer nature at ca. 560 nm at 298 K (Figure 7A) [55]. Complexes E-**1Ag** and Z-**1Ag** demonstrate practically the same maxima. A temperature decrease leads to the shifting of maxima of the initial Z-**1** and E-**1** to 605 and 575 nm, respectively (Figure 7B). Complexes E-**1Ag** and Z-**1Ag** demonstrate structured bands centered at 580 and 590 nm (Figure 7B). Complexation leads to the changing of the emission profile only at low temperatures. It could be assigned to the arising effect of the silver ions only at 77 K. It is known that silver pyrazolate adducts commonly emit light only at low temperatures [53]. In contrast, the complexation leads to the structured emissions that are typical for the $\pi\rightarrow\pi^*/n\rightarrow\pi^*$ emission of extended π-electronic systems (Figure 7B). Chalcone E-**2** exhibits non-intense structured emission of $\pi\rightarrow\pi^*/n\rightarrow\pi^*$ nature (Figure 7C). Complexation leads to the shifting of the emission to the low-energy region (maxima 620 nm). The observed emission is near to the observed for complex E-**1Ag** demonstrating the same structure of the chalcone. It could be assigned to a similar emission with the silver ion effect.

Table 2. ^{13}C NMR chemical shifts of E-**1** and Z-**1** in the presence of different amounts of $[AgPz]_3$, CCl_4/C_6D_6 (v/v = 9/1), 298 K.

		E-**1**(δ, ppm)	+ $[AgPz]_3$ (Δδ, ppm)	Z-**1** (δ, ppm)	+ $[AgPz]_3$ (Δδ, ppm)
C=O	3	187.51	−0.17	187.73	+0.66
Py	4	154.34	+0.04	154.29	−0.59
	5	148.63	+0.62	148.27	+0.19
	6	128.10	+0.15	126.69	−0.10
	7	136.37	+0.33	136.14	−0.07
	8	122.82	+0.48	122.30	+0.21
C=C	1	140.85	+0.08	140.55	−0.65
	2	130.63	−0.6	131.17	−0.27
Anthracene	9	131.32	−0.26	131.78	−0.15
	10	128.66	−0.16	128.30	+0.08
	11	126.07	+0.55	125.75	−0.26
	12	125.12	−0.11	124.81	+0.31
	13	125.67	−0.18	125.22	+0.27
	14	130.00	−0.18	128.66	+0.03
	15	129.85	−0.24	128.63	−0.04
	16	126.20	+0.42	125.94	+0.13

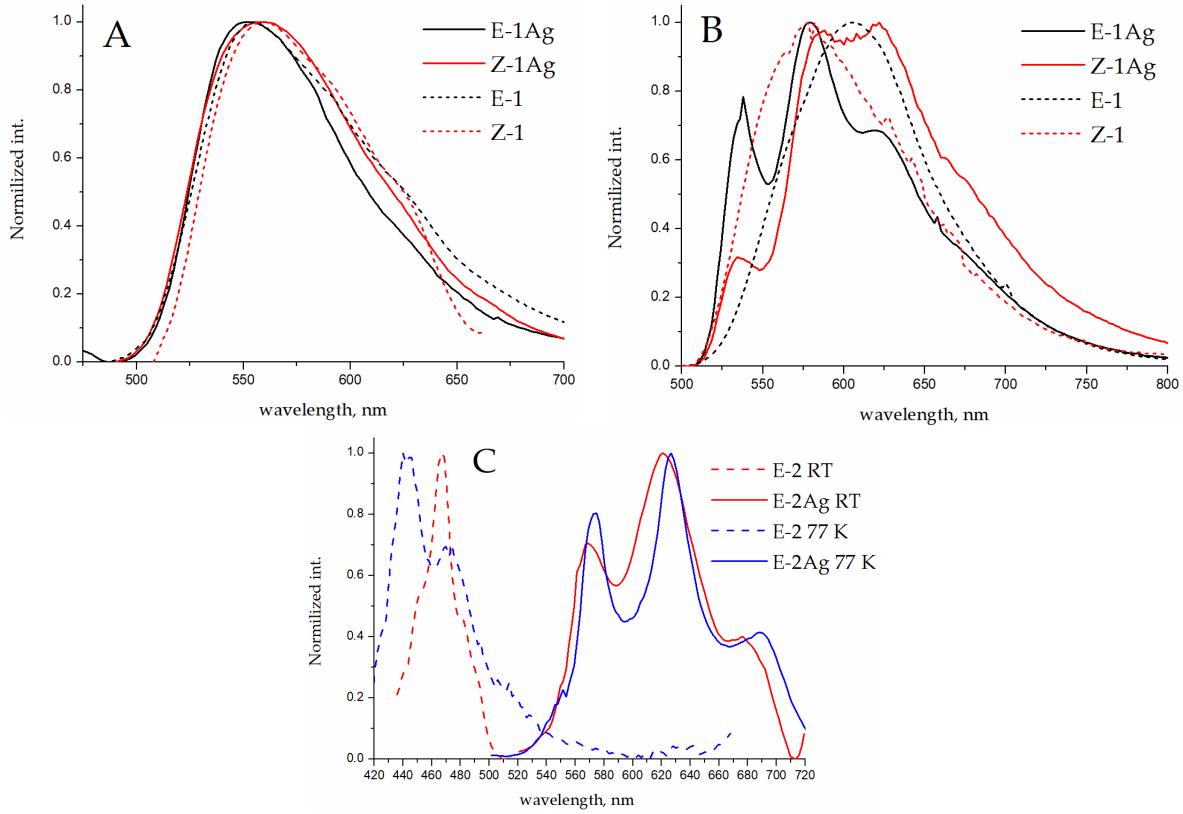


Figure 7. Normalized emission spectra of the solid samples (λ_{exc} = 340 nm) E-**1**, Z-**1** (dashed lines) and their complexes **E-1Ag, Z-1Ag** (solid lines) at 298 K (**A**) and 77 K (**B**). Normalized emission spectra of the solid samples (λ_{exc} = 340 nm) E-**2** (dashed lines) and **E-2Ag** (solid lines) at 298 and 77K (**C**).

3. Materials and Methods

3.1. Physical Measurement and Instrumentation

^{1}H and ^{13}C NMR measurements were carried out on Bruker Avance 400 (Bruker). Infrared (IR) spectra were collected on a Shimadzu IRPrestige 21 FT-IR spectrometer in KBr pellets (Shimadzu, Kyoto, Japan). The UV-vis spectra of solutions were measured on Cary 50 (Varian, Palo Alto, CA, USA). The photoluminescence spectra in the solution were measured on Shimadzu RF-6000 (Shimadzu, Kyoto, Japan). The samples for these measurements were packed in quartz capillaries.

3.2. Crystal Structure Determination

Single-crystal X-ray diffraction experiments were carried out with a Bruker SMART APEX II diffractometer (Bruker). The APEX II software [56] was used for collecting frames of data, indexing reflections, determination of lattice constants, integration of intensities of reflections, scaling, and absorption correction. The structures were solved by a dual-space algorithm and refined in anisotropic approximation for non-hydrogen atoms against F 2 (hkl). Hydrogen atoms were calculated according to the idealized geometries and refined with constraints applied to C-H and N-H bond lengths and equivalent displacement parameters (U eq (H) = 1.2U eq (X), X denotes central atom of XH_2 group; U eq (H) = 1.5U eq (Y), Y denotes central atom of YH_3 group). All structures were solved with the ShelXT [57] program and refined with the ShelXL [58] program. Molecular graphics were drawn using OLEX2 [59] program. CCDC 2252898-2252900 contains the supplementary crystallographic data for this paper. These data can be obtained free of charge from the Cambridge Crystallographic Data Centre.

3.3. Computational Details

The DFT computations were performed with the ORCA 5.03 package [60,61], applying ωB97X-D3 functional [62,63] and the def2-TZVP [64] basis set with the ZORA relativistic Hamiltonian. The ground states were fully optimized without any constraints. The RIJCOSX procedure was used to speed up calculations.

3.4. Synthesis and Characterization

All reactions were performed under an argon atmosphere using anhydrous solvents or solvents treated with an appropriate drying reagent. The chalcones [55] and $[MPz]_3$ [65] were synthesized as described.

4. Conclusions

The investigation of the interaction of $[AgPz]_3$ with pyridine-substituted chalcones allows us to establish the general features of the structure, the sites of coordination, and the role of E-Z isomerization on the complexes' formation. The non-covalent π-π/M-π interactions play a key role in the formation of complexes of pyridine-based chalcones with the trinuclear silver(I) pyrazolate even in the presence of pyridine fragments and carbonyl groups. It is shown that chalcones in E-isomeric form seek to planar structure in the complexes with trinuclear pyrazolate adduct $[AgPz]_3$ via multiple π-π/M-π. Carbonyl and pyridine fragments also take place in coordination with the $[AgPz]_3$. In contrast, **Z-1** chalcone coordinates to silver(I) macrocycle via the chelating of metal ions by O- and N atoms. The results of the DFT calculation show the presence of possible eight isomers/conformers of 3-(anthracen-9-yl)-1-(pyridin-2-yl)prop-2-en-1-one interpreting the complicated IR-spectral behavior. These data demonstrate the non-possibility of establishing quantitative characteristics of the complexes obtained due to the presence of several bands. However, shifts of IR-spectral bands as well as NMR resonances demonstrate the preferable coordination of the carbonyl group with the silver ions in Z-isomers. The spectral data suggest retaining the structures for all studied complexes in solution and solid state. The complexation in the case of anthracene-containing chalcones allows the switching of the emission nature from charge-transfer to ligand-centered at 77 K. In contrast,

in the case of phenyl-containing chalcone, possessing only $\pi\rightarrow\pi^*/n\rightarrow\pi^*$ transitions, the complexes formation leads to the significant emission (Δ = ca. 155 nm) shifting to the low-energy region.

Supplementary Materials: The following supporting information can be downloaded at: https://www.mdpi.com/article/10.3390/inorganics11040175/s1. Scheme S1: Possible isomers for pyridine-chalcones.; Scheme S2: Schematic representation of supramolecular packing of E-**1Ag** and E-**2Ag**; Scheme S3: Schematic representation of supramolecular packing of Z-**1Ag**; Table S1: Crystal data, data collection, and structure refinement parameters for E-**1Ag**, E-**2Ag** Z-**1Ag**; **Figure S1**: ^{1}H NMR spectrum of E-**1** in the mixture CCl_4/benzene-d6 (9/1); Figure S2: ^{13}C NMR spectrum of E-**1** in CCl_4/benzene-d_6 (9/1) mixture; Figure S3: ^{1}H NMR spectrum of E-**1** + 1 eq. $[AgPz]_3$ in CCl_4/benzene-d_6 (9/1) mixture; Figure S4: ^{13}C NMR spectrum of E-**1** + 1 eq. $[AgPz]_3$ in CCl_4/benzene-d_6 (9/1) mixture; Figure S5: ^{1}H NMR spectrum of Z-**1** in CCl_4/benzene-d_6 (9/1) mixture; Figure S6: ^{13}C NMR spectrum of Z-**1** in CCl_4/benzene-d_6 (9/1) mixture; Figure S7: ^{1}H NMR spectrum of Z-**1** + 0.5 eq. $[AgPz]_3$ in CCl_4/benzene-d_6 (9/1) mixture; Figure S8: ^{13}C NMR spectrum of Z-**1** + 0.5 eq. $[AgPz]_3$ in CCl_4/benzene-d_6 (9/1) mixture; Figure S9: IR spectra of E-**1** in KBr; Figure S10: IR spectra of **E-1Ag** in KBr; Figure S11: IR spectra of Z-**1** in KBr; Figure S12: IR spectra of **Z-1Ag** in KBr; Figure S13: IR spectra of E-**2** in KBr; Figure S14: IR spectra of E-**2Ag** in KBr; Figure S15: UV-vis spectra of E-**1** + $[AgPz]_3$ c = 0.015, d = 0.047 mm in CCl_4; Figure S16: UV-vis spectra of Z-**1** + $[AgPz]_3$, c = 0.015, d = 0.047 mm in CCl_4; Figure S17: UV-vis spectra of E-**1** + $[AgPz]_3$ c = 0.015 d = 0.047 mm in CCl_4; Figure S18: The Job's plot: dependence of the $\nu(CO)^{bond}$ band intensity of $[AgPz]_3$*[Z-**1**] (1674 cm^{-1}) on the composition of the isomolar solution of E-**1** and $[AgPz]_3$, CCl_4; Figure S19: Simulated IR spectra for conformers of chalcone E-**1**. Frequency scales by 0.950, FWHH set to 19.

Author Contributions: Investigation, formal analysis, A.O.; formal analysis, investigation, writing original draft, A.T.; investigation, resources, A.S.; software, methodology, writing review and editing, funding acquisition, O.F.; writing review and editing, E.S.S. All authors have read and agreed to the published version of the manuscript.

Funding: This work was financially supported by the Russian Science Foundation (project No 19-73-20262).

Institutional Review Board Statement: Not applicable.

Informed Consent Statement: Not applicable.

Data Availability Statement: The data presented in this study are available in article and supplementary materials.

Acknowledgments: NMR and XRD measurements were performed using the equipment of the Center for Molecular Composition Studies at the INEOS RAS and were supported by the Ministry of Science and Higher Education of the Russian Federation.

Conflicts of Interest: The authors declare no conflict of interest.

References

1. Mahmudov, K.T.; Kopylovich, M.N.; Guedes da Silva, M.F.C.; Pombeiro, A.J.L. Non-covalent interactions in the synthesis of coordination compounds: Recent advances. *Coord. Chem. Rev.* **2017**, *345*, 54–72. [CrossRef]
2. Alkorta, I.; Elguero, J.; Frontera, A. Not Only Hydrogen Bonds: Other Noncovalent Interactions. *Crystals* **2020**, *10*, 180. [CrossRef]
3. Cornaton, Y.; Djukic, J.P. Noncovalent Interactions in Organometallic Chemistry: From Cohesion to Reactivity, a New Chapter. *Acc. Chem. Res.* **2021**, *54*, 3828–3840. [CrossRef] [PubMed]
4. Yang, J.; Zhen, X.; Wang, B.; Gao, X.; Ren, Z.; Wang, J.; Xie, Y.; Li, J.; Peng, Q.; Pu, K.; et al. The influence of the molecular packing on the room temperature phosphorescence of purely organic luminogens. *Nat. Commun.* **2018**, *9*, 840. [CrossRef] [PubMed]
5. Zhou, B.; Yan, D. Hydrogen-Bonded Two-Component Ionic Crystals Showing Enhanced Long-Lived Room-Temperature Phosphorescence via TADF-Assisted Förster Resonance Energy Transfer. *Adv. Funct. Mater.* **2019**, *29*, 1807599. [CrossRef]
6. Wang, W.; Zhang, Y.; Jin, W.J. Halogen bonding in room-temperature phosphorescent materials. *Coord. Chem. Rev.* **2020**, *404*, 213107. [CrossRef]
7. McNaughton, D.A.; Fares, M.; Picci, G.; Gale, P.A.; Caltagirone, C. Advances in fluorescent and colorimetric sensors for anionic species. *Coord. Chem. Rev.* **2021**, *427*, 213573. [CrossRef]

8. El Sayed Moussa, M.; Evariste, S.; Wong, H.L.; Le Bras, L.; Roiland, C.; Le Polles, L.; Le Guennic, B.; Costuas, K.; Yam, V.W.; Lescop, C. A solid state highly emissive Cu(i) metallacycle: Promotion of cuprophilic interactions at the excited states. *Chem. Commun.* **2016**, *52*, 11370–11373. [CrossRef]
9. Liu, W.; Zhu, K.; Teat, S.J.; Dey, G.; Shen, Z.; Wang, L.; O'Carroll, D.M.; Li, J. All-in-One: Achieving Robust, Strongly Luminescent and Highly Dispersible Hybrid Materials by Combining Ionic and Coordinate Bonds in Molecular Crystals. *J. Am. Chem. Soc.* **2017**, *139*, 9281–9290. [CrossRef]
10. Baranov, A.Y.; Pritchina, E.A.; Berezin, A.S.; Samsonenko, D.G.; Fedin, V.P.; Belogorlova, N.A.; Gritsan, N.P.; Artem'ev, A.V. Beyond Classical Coordination Chemistry: The First Case of a Triply Bridging Phosphine Ligand. *Angew. Chem. Int. Ed. Engl.* **2021**, *60*, 12577–12584. [CrossRef]
11. Rogovoy, M.I.; Berezin, A.S.; Samsonenko, D.G.; Artem'ev, A.V. Silver(I)-Organic Frameworks Showing Remarkable Thermo-, Solvato- And Vapochromic Phosphorescence As Well As Reversible Solvent-Driven 3D-to-0D Transformations. *Inorg. Chem.* **2021**, *60*, 6680–6687. [CrossRef] [PubMed]
12. Demyanov, Y.V.; Sadykov, E.H.; Rakhmanova, M.I.; Novikov, A.S.; Bagryanskaya, I.Y.; Artem'ev, A.V. Tris(2-Pyridyl)Arsine as a New Platform for Design of Luminescent Cu(I) and Ag(I) Complexes. *Molecules* **2022**, *27*, 6059. [CrossRef] [PubMed]
13. Housecroft, C.E.; Constable, E.C. TADF: Enabling luminescent copper(i) coordination compounds for light-emitting electrochemical cells. *J. Mater. Chem. C Mater.* **2022**, *10*, 4456–4482. [CrossRef] [PubMed]
14. Yersin, H.; Czerwieniec, R.; Monkowius, U.; Ramazanov, R.; Valiev, R.; Shafikov, M.Z.; Kwok, W.-M.; Ma, C. Intersystem crossing, phosphorescence, and spin-orbit coupling. Two contrasting Cu(I)-TADF dimers investigated by milli- to micro-second phosphorescence, femto-second fluorescence, and theoretical calculations. *Coord. Chem. Rev.* **2023**, *478*, 214975. [CrossRef]
15. Cui, Y.; Li, B.; He, H.; Zhou, W.; Chen, B.; Qian, G. Metal-Organic Frameworks as Platforms for Functional Materials. *Acc. Chem. Res.* **2016**, *49*, 483–493. [CrossRef]
16. Lin, R.B.; Liu, S.Y.; Ye, J.W.; Li, X.Y.; Zhang, J.P. Photoluminescent Metal-Organic Frameworks for Gas Sensing. *Adv. Sci.* **2016**, *3*, 1500434. [CrossRef] [PubMed]
17. Huang, C.H.; Yang, M.; Chen, X.L.; Lu, C.Z. Bright bluish-green emitting Cu(I) complexes exhibiting efficient thermally activated delayed fluorescence. *Dalton Trans.* **2021**, *50*, 5171–5176. [CrossRef]
18. Wang, Y.-N.; Wang, S.-D.; Lv, J.-H.; Cao, K.-Z.; Liu, H.-Q.; Wang, F.; Lu, S.-Q. Novel nickel(II) coordination polymer based on a semi-rigid tricarboxylate acid ligand: Synthesis, structure, and fluorescence recognition of acetylacetone in aqueous media. *J. Mol. Struct.* **2022**, *1247*, 131317. [CrossRef]
19. Zhu, M.; Chen, J.; Guo, R.; Xu, J.; Fang, X.; Han, Y.-F. Cobalt phthalocyanine coordinated to pyridine-functionalized carbon nanotubes with enhanced CO_2 electroreduction. *Appl. Catal. B Environ.* **2019**, *251*, 112–118. [CrossRef]
20. Olivo, G.; Capocasa, G.; Del Giudice, D.; Lanzalunga, O.; Di Stefano, S. New horizons for catalysis disclosed by supramolecular chemistry. *Chem. Soc. Rev.* **2021**, *50*, 7681–7724. [CrossRef]
21. Larionov, V.A.; Feringa, B.L.; Belokon, Y.N. Enantioselective "organocatalysis in disguise" by the ligand sphere of chiral metal-templated complexes. *Chem. Soc. Rev.* **2021**, *50*, 9715–9740. [CrossRef] [PubMed]
22. Titov, A.A.; Filippov, O.A.; Epstein, L.M.; Belkova, N.V.; Shubina, E.S. Macrocyclic copper(I) and silver(I) pyrazolates: Principles of supramolecular assemblies with Lewis bases. *Inorg. Chim. Acta* **2018**, *470*, 22–35. [CrossRef]
23. Zheng, J.; Yang, H.; Xie, M.; Li, D. The pi-acidity/basicity of cyclic trinuclear units (CTUs): From a theoretical perspective to potential applications. *Chem. Commun.* **2019**, *55*, 7134–7146. [CrossRef]
24. Zheng, J.; Lu, Z.; Wu, K.; Ning, G.H.; Li, D. Coinage-Metal-Based Cyclic Trinuclear Complexes with Metal-Metal Interactions: Theories to Experiments and Structures to Functions. *Chem. Rev.* **2020**, *120*, 9675–9742. [CrossRef]
25. Dias, H.V.R.; Diyabalanage, H.V.K.; Rawashdeh-Omary, M.A.; Franzman, M.A.; Omary, M.A. Bright Phosphorescence of a Trinuclear Copper(I) Complex: Luminescence Thermochromism, Solvatochromism, and "Concentration Luminochromism". *J. Am. Chem. Soc.* **2003**, *125*, 12072–12073. [CrossRef] [PubMed]
26. Dias, H.V.; Diyabalanage, H.V.; Eldabaja, M.G.; Elbjeirami, O.; Rawashdeh-Omary, M.A.; Omary, M.A. Brightly phosphorescent trinuclear copper(I) complexes of pyrazolates: Substituent effects on the supramolecular structure and photophysics. *J. Am. Chem. Soc.* **2005**, *127*, 7489–7501. [CrossRef] [PubMed]
27. Parasar, D.; Ponduru, T.T.; Noonikara-Poyil, A.; Jayaratna, N.B.; Dias, H.V.R. Acetylene and terminal alkyne complexes of copper(I) supported by fluorinated pyrazolates: Syntheses, structures, and transformations. *Dalton Trans.* **2019**, *48*, 15782–15794. [CrossRef]
28. Titov, A.A.; Larionov, V.A.; Smol'yakov, A.F.; Godovikova, M.I.; Titova, E.M.; Maleev, V.I.; Shubina, E.S. Interaction of a trinuclear copper(I) pyrazolate with alkynes and carbon-carbon triple bond activation. *Chem. Commun.* **2019**, *55*, 290–293. [CrossRef]
29. Yang, L.; Wang, L.; Lv, X.; Chen, J.H.; Wang, Y.; Yang, G. Complexation of triangular silver(I) or copper(I) nitropyrazolates with dibenzothiophenes having potential use in adsorptive desulfurization. *Dalton Trans.* **2021**, *50*, 2915–2927. [CrossRef]
30. Larionov, V.A.; Stashneva, A.R.; Titov, A.A.; Lisov, A.A.; Medvedev, M.G.; Smol'yakov, A.F.; Tsedilin, A.M.; Shubina, E.S.; Maleev, V.I. Mechanistic study in azide-alkyne cycloaddition (CuAAC) catalyzed by bifunctional trinuclear copper(I) pyrazolate complex: Shift in rate-determining step. *J. Catal.* **2020**, *390*, 37–45. [CrossRef]
31. Zheng, J.; Wang, J.N.; Wang, T.; Wu, K.; Wei, R.J.; Lu, W.G.; Li, D. Phosphorescent Metal Rotaxane-like Bimetallic Ag/Au Clusters. *J. Phys. Chem. C* **2021**, *125*, 9400–9410. [CrossRef]

32. Zhang, M.-M.; Dong, X.-Y.; Wang, Y.-J.; Zang, S.-Q.; Mak, T.C.W. Recent progress in functional atom-precise coinage metal clusters protected by alkynyl ligands. *Coord. Chem. Rev.* **2022**, *453*, 214315. [CrossRef]
33. Morishima, Y.; Young, D.J.; Fujisawa, K. Structure and photoluminescence of silver(i) trinuclear halopyrazolato complexes. *Dalton Trans.* **2014**, *43*, 15915–15928. [CrossRef] [PubMed]
34. Chen, J.H.; Liu, Y.M.; Zhang, J.X.; Zhu, Y.Y.; Tang, M.S.; Ng, S.W.; Yang, G. Halogen-involving weak interactions manifested in the crystal structures of silver(I) or gold(I) 4-halogenated-3,5-diphenylpyrazolato trimers. *Crystengcomm* **2014**, *16*, 4987–4998. [CrossRef]
35. Titov, A.A.; Guseva, E.A.; Filippov, O.A.; Babakhina, G.M.; Godovikov, I.A.; Belkova, N.V.; Epstein, L.M.; Shubina, E.S. The Role of Weak Interactions in Strong Intermolecular M...Cl Complexes of Coinage Metal Pyrazolates: Spectroscopic and DFT Study. *J. Phys. Chem. A* **2016**, *120*, 7030. [CrossRef]
36. Zhan, S.Z.; Li, M.; Zheng, J.; Wang, Q.J.; Ng, S.W.; Li, D. Luminescent Cu_4I_4-Cu_3(Pyrazolate)$_3$ Coordination Frameworks: Postsynthetic Ligand Substitution Leads to Network Displacement and Entanglement. *Inorg. Chem.* **2017**, *56*, 13446–13455. [CrossRef]
37. Zhan, S.Z.; Jiang, X.; Zheng, J.; Huang, X.D.; Chen, G.H.; Li, D. A luminescent supramolecular $Cu_2I_2(NH_3)_2$-sandwiched Cu_3(pyrazolate)$_3$ adduct as a temperature sensor. *Dalton Trans.* **2018**, *47*, 3679–3683. [CrossRef]
38. Omary, M.A.; Rawashdeh-Omary, M.A.; Diyabalanage, H.V.; Dias, H.V. Blue phosphors of dinuclear and mononuclear copper(I) and silver(I) complexes of 3,5-bis(trifluoromethyl)pyrazolate and the related bis(pyrazolyl)borate. *Inorg. Chem.* **2003**, *42*, 8612. [CrossRef]
39. Yang, C.; Elbjeirami, O.; Gamage, C.S.P.; Dias, H.V.R.; Omary, M.A. Luminescence enhancement and tuning via multiple cooperative supramolecular interactions in an ion-paired multinuclear complex. *Chem. Commun.* **2011**, *47*, 7434–7436. [CrossRef]
40. Titov, A.A.; Smol'yakov, A.F.; Baranova, K.F.; Filippov, O.A.; Shubina, E.S. Synthesis, structures and photophysical properties of phosphorus-containing silver 3,5-bis(trifluoromethyl)pyrazolates. *Mendeleev Commun.* **2018**, *28*, 387–389. [CrossRef]
41. Titov, A.A.; Filippov, O.A.; Smol'yakov, A.F.; Baranova, K.F.; Titova, E.M.; Averin, A.A.; Shubina, E.S. Dinuclear CuI and AgI Pyrazolates Supported with Tertiary Phosphines: Synthesis, Structures, and Photophysical Properties. *Eur. J. Inorg. Chem.* **2019**, *2019*, 821–827. [CrossRef]
42. Titov, A.A.; Filippov, O.A.; Smol'yakov, A.F.; Averin, A.A.; Shubina, E.S. Synthesis, structures and luminescence of multinuclear silver(i) pyrazolate adducts with 1,10-phenanthroline derivatives. *Dalton Trans.* **2019**, *48*, 8410–8417. [CrossRef] [PubMed]
43. Yakovlev, G.B.; Titov, A.A.; Smol'yakov, A.F.; Chernyadyev, A.Y.; Filippov, O.A.; Shubina, E.S. Tetranuclear Copper(I) and Silver(I) Pyrazolate Adducts with 1,1′-Dimethyl-2,2′-bibenzimidazole: Influence of Structure on Photophysics. *Molecules* **2023**, *28*, 1189. [CrossRef] [PubMed]
44. Titov, A.A.; Smol'yakov, A.F.; Filippov, O.A. Heterobimetallic Silver(I) and Copper(I) pyrazolates supported with 1,1′-bis(diphenylphosphino)ferrocene. *J. Organomet. Chem.* **2021**, *942*, 121813. [CrossRef]
45. Titov, A.A.; Filippov, O.A.; Guseva, E.A.; Smol'yakov, A.F.; Dolgushin, F.M.; Epstein, L.M.; Belsky, V.K.; Shubina, E.S. Role of basic sites of substituted ferrocenes in interaction with the trinuclear 3,5-bis(trifluoromethyl)pyrazolates: Thermodynamics and structure of complexes. *RSC Adv.* **2014**, *4*, 8350. [CrossRef]
46. Titov, A.A.; Smol'yakov, A.F.; Godovikov, I.A.; Chernyadyev, A.Y.; Molotkov, A.P.; Loginov, D.A.; Filippov, O.A.; Belkova, N.V.; Shubina, E.S. The role of weak intermolecular interactions in photophysical behavior of isocoumarins on the example of their interaction with cyclic trinuclear silver(I) pyrazolate. *Inorg. Chim. Acta* **2022**, *539*, 121004. [CrossRef]
47. Nongbri, S.L.; Das, B.; Rao, K.M. Isolation and spectral studies of water-soluble η^5-cyclichydrocarbon rhodium and iridium complexes with pyridyl diketone analogues bonded through κ^2-N∩O,κ^4–N∩O, and κ^3-N-C-N modes. *J. Coord. Chem.* **2012**, *65*, 875–890. [CrossRef]
48. Zhang, H.-N.; Wang, J.; Hu, H.-M.; Yuan, F.; Song, J.; Xue, G.-L. Crystal Structures and Luminescent Properties of Two Zinc(II) Coordination Compounds with a β-Diketonate Derivative Ligand. *Z. Anorg. Allg. Chem.* **2013**, *639*, 1850–1854. [CrossRef]
49. Balázs, L.B.; Tay, W.S.; Li, Y.; Pullarkat, S.A.; Leung, P.-H. Synthesis of Stereoprojecting, Chiral N-C(sp^3)-E Type Pincer Complexes. *Organometallics* **2018**, *37*, 2272–2285. [CrossRef]
50. Thomas, J.M.; Kuduvalli, S.S.; Anitha, T.S.; Sivasankar, C. Investigation of the CO releasing ability of azachalcone bound Mn(I) tricarbonyl complexes and their antiproliferative properties. *Appl. Organomet. Chem.* **2022**, *36*, 6896. [CrossRef]
51. Alecu, I.M.; Zheng, J.; Zhao, Y.; Truhlar, D.G. Computational Thermochemistry: Scale Factor Databases and Scale Factors for Vibrational Frequencies Obtained from Electronic Model Chemistries. *J. Chem. Theory Comput.* **2010**, *6*, 2872–2887. [CrossRef]
52. Constable, E.C.; Smith, D.R. Photoisomerisation of 9-anthrylsubstituted pyridyl enones. *Tetrahedron* **1996**, *52*, 935–940. [CrossRef]
53. Titov, A.A.; Smol'yakov, A.F.; Filippov, O.A.; Godovikov, I.A.; Muratov, D.A.; Dolgushin, F.M.; Epstein, L.M.; Shubina, E.S. Supramolecular Design of the Trinuclear Silver(I) and Copper(I) Metal Pyrazolates Complexes with Ruthenium Sandwich Compounds via Intermolecular Metal−π Interactions. *Cryst. Growth Des.* **2017**, *17*, 6770–6779. [CrossRef]
54. Duraimurugan, K.; Harikrishnan, M.; Madhavan, J.; Siva, A.; Lee, S.J.; Theerthagiri, J.; Choi, M.Y. Anthracene-based fluorescent probe: Synthesis, characterization, aggregation-induced emission, mechanochromism, and sensing of nitroaromatics in aqueous media. *Environ. Res.* **2021**, *194*, 110741. [CrossRef] [PubMed]
55. Omary, M.A.; Rawashdeh-Omary, M.A.; Gonser, M.W.A.; Elbjeirami, O.; Grimes, T.; Cundari, T.R.; Diyabalanage, H.V.K.; Gamage, C.S.P.; Dias, H.V.R. Metal Effect on the Supramolecular Structure, Photophysics, and Acid−Base Character of Trinuclear Pyrazolato Coinage Metal Complexes. *Inorg. Chem.* **2005**, *44*, 8200–8210. [CrossRef] [PubMed]

56. *APEX II software Package*; Bruker AXS Inc.: Madison, WI, USA, 2005.
57. Sheldrick, G. SHELXT—Integrated space-group and crystal-structure determination. *Acta Crystallogr. Sect. A* **2015**, *71*, 3–8. [CrossRef] [PubMed]
58. Sheldrick, G. Crystal structure refinement with SHELXL. *Acta Crystallogr. Sect. C* **2015**, *71*, 3–8. [CrossRef]
59. Dolomanov, O.V.; Bourhis, L.J.; Gildea, R.J.; Howard, J.A.K.; Puschmann, H. OLEX2: A complete structure solution, refinement and analysis program. *J. Appl. Crystallogr.* **2009**, *42*, 339–341. [CrossRef]
60. Neese, F. Software update: The ORCA program system, version 4.0. *WIREs Comput. Mol. Sci.* **2018**, *8*, e1327. [CrossRef]
61. Neese, F. The ORCA program system. *WIREs Comput. Mol. Sci.* **2011**, *2*, 73–78. [CrossRef]
62. Grimme, S.; Antony, J.; Ehrlich, S.; Krieg, H. A consistent and accurate ab initio parametrization of density functional dispersion correction (DFT-D) for the 94 elements H-Pu. *J. Chem. Phys.* **2010**, *132*, 154104. [CrossRef] [PubMed]
63. Lin, Y.S.; Li, G.D.; Mao, S.P.; Chai, J.D. Long-Range Corrected Hybrid Density Functionals with Improved Dispersion Corrections. *J. Chem. Theory Comput.* **2013**, *9*, 263–272. [CrossRef] [PubMed]
64. Weigend, F.; Ahlrichs, R. Balanced basis sets of split valence, triple zeta valence and quadruple zeta valence quality for H to Rn: Design and assessment of accuracy. *Phys. Chem. Chem. Phys.* **2005**, *7*, 3297–3305. [CrossRef] [PubMed]
65. Rasika Dias, H.V.; Polach, S.A.; Wang, Z. Coinage metal complexes of 3,5-bis(trifluoromethyl)pyrazolate ligand: Synthesis and characterization of $\{[3,5\text{-}(CF_3)_2Pz]Cu\}_3$ and $\{[3,5\text{-}(CF_3)_2Pz]Ag\}_3$. *J. Fluor. Chem.* **2000**, *103*, 163–169. [CrossRef]

Disclaimer/Publisher's Note: The statements, opinions and data contained in all publications are solely those of the individual author(s) and contributor(s) and not of MDPI and/or the editor(s). MDPI and/or the editor(s) disclaim responsibility for any injury to people or property resulting from any ideas, methods, instructions or products referred to in the content.